

### **Geocarto International**



ISSN: 1010-6049 (Print) 1752-0762 (Online) Journal homepage: www.tandfonline.com/journals/tgei20

# Assessment of multi-sensor approach to savanna landscape mapping in Ghana

Kenneth Aidoo, Ferdinand Tornyie, Fatima Denton, Ursula Gessner & Alex Barimah Owusu

**To cite this article:** Kenneth Aidoo, Ferdinand Tornyie, Fatima Denton, Ursula Gessner & Alex Barimah Owusu (2025) Assessment of multi-sensor approach to savanna landscape mapping in Ghana, Geocarto International, 40:1, 2555444, DOI: 10.1080/10106049.2025.2555444

To link to this article: <a href="https://doi.org/10.1080/10106049.2025.2555444">https://doi.org/10.1080/10106049.2025.2555444</a>

9	© 2025 The Author(s). Published by Informa UK Limited, trading as Taylor & Francis Group
	Published online: 29 Sep 2025.
	Submit your article to this journal $oldsymbol{oldsymbol{\mathcal{C}}}$
hh	Article views: 221
Q	View related articles 🗗
CrossMark	View Crossmark data 🗗



**3** OPEN ACCESS



## Assessment of multi-sensor approach to savanna landscape mapping in Ghana

Kenneth Aidoo<sup>a,b</sup>, Ferdinand Tornyie<sup>a</sup>, Fatima Denton<sup>a</sup>, Ursula Gessner<sup>c</sup> and Alex Barimah Owusu<sup>b</sup>

<sup>a</sup>United Nations University, Institute for Natural Resources in Africa (UNU-INRA), Accra, Ghana; <sup>b</sup>Department of Geography and Resource Development, University of Ghana, Accra, Ghana; <sup>c</sup>German Aerospace Center (DLR), German Remote Sensing Data Center (DFD), Oberpfaffenhofen, Germany

#### **ABSTRACT**

Land Use Land Cover (LULC) maps play an important role in land cover change assessment. In this study existing LULC maps of 2006 and 2015 were used to develop a standardized LULC classification procedure for continuous mapping and land management. The same procedure was used to produce 2023 LULC map for the study area. Landsat 8, Sentinel-1, and Sentinel-2 were used in combination with a Random Forest algorithm to assess the potential of multi-sensor Earth observations in mapping savanna ecological zones in the Google Earth Engine (GEE). The classification results yielded an overall accuracy of 73.32% and kappa coefficient of 0.6342 when integrating Landsat 8 and Sentinel-2 data. In addition, an overall accuracy of 80.21% and kappa coefficient of 0.7225 were obtained for the combined Landsat 8, Sentinel-2, and Sentinel-1 data. The results demonstrated that using Sentinel-1 data in addition to multispectral data improved the classification accuracy by almost 7%.

#### ARTICLE HISTORY

Received 22 June 2025 Accepted 27 August 2025

#### **KEYWORDS**

Land use land cover; savanna ecological zone; multi-sensor; random forest; Google earth engine

#### 1. Introduction

Land is an essential natural resource that supports the human population in the savannas of sub-Saharan Africa (Mbow 2020). The impact of the utilization is evident in rural areas where the population relies heavily on natural resources on the land to meet their energy and nutrition needs (Antwi et al. 2014; Onyeaka et al. 2024). The environment and thus the ecosystem, bears the full brunt of human activities by the conversion of savanna or forest vegetation to human dominated landscapes (Osborne et al. 2018). This is in the form of deforestation, pollution of fresh water bodies, and drainage of wetlands, culminating in habitat loss, expansion of cropland, and opening up spaces for settlements (Repetto and Holmes 1983).

The anthropogenic disturbances on the savanna landscape are scattered and vary depending on the season and the socioeconomic factors driving it, resulting in landscape degradation (Baade et al. 2021; Jorge et al. 2025). It is difficult to monitor these variable disturbances for a comprehensive understanding of their impact on the savanna landscape. Thus, it is challenging to understand the linkage of ever-changing land cover at disturbed and undisturbed locations from a local perspective (Grégoire et al. 2013; Biah et al. 2024). With increasing demands to keep abreast with changing Land Use Land Cover (LULC) in savanna landscapes, there is, therefore the need to model an approach to accurately take inventory of savanna landscapes as a whole for easy and quick understanding of changing trends in vegetation cover.

Although, some LULC classifications have been produced or created for the five savanna dominated northern regions in Ghana, there are still gaps or drawbacks in the analysis conducted thus far. This has to do with the data used in producing LULC maps, as many studies derived their land cover classes from the training data they acquired and were not based on any previous work that has been done. Few studies have attempted to produce LULC maps with sample data based on harmonized historic LULC maps consistent with the Land Cover Classification System (LCCS) defined by the Food and Agriculture Organization of the United Nations (FAO) and the United Nations Environment Programme (UNEP) as the reference classification system for data collection (Gregorio and Jansen 2000) and with reference to the translatability of land cover classes in the International Geosphere–Biosphere Program (IGBP) (Gregorio et al. 2016) to improve or update previous LULC maps for accurate land cover inventories.

The growing demand for LULC maps to replace or update existing maps has created the opportunity for advances in classification approaches to be applied in several landscapes to address issues of land cover changes at local, regional, and global scales. These demands have led to advances in machine learning (ML) algorithms with varying degree of accuracy but Random Forest (RF) and Support Vector Machine (SVM) have been highlighted as having outstanding performance compared to their counterparts in numerous literature (Mountrakis et al. 2011; Belgiu and Drăguţ 2016; Sheykhmousa et al. 2020). RF is an ensemble learning model that builds decision trees using random samples of observations and variables. The output is an assignment of the class selected by the majority of the decision trees. The RF further provides a score called feature importance to depict the relevance of each predictor within the model. By building multiple trees, the RF can correct the decision tree problem of overfitting. (Chabi et al. 2016; Zoungrana and Dimobé 2023).

Support Vector Machine (SVM) is supervised machine learning algorithms applied in remote sensing for classification tasks. The fundamental of SVM is to identify an optimal decision boundary, refer to as a hyperplane, separating data points into distinct classes. During the training process, the algorithm assigns each data point to a specific category, thereby functioning as a binary linear classifier. As a non-parametric supervised model, SVM does not rely on assumptions about the underlying data distribution, making it robust to variations in data characteristics (Mountrakis et al. 2011). This property provides a significant advantage over parametric classification methods, which require such distributional assumptions.

This study employed Earth observation techniques to monitor savanna landscapes and harmonize existing land use/land cover (LULC) maps for the five northern regions of Ghana. The analysis was conducted using Google Earth Engine (GEE), a planetaryscale cloud platform for Earth science data processing and analysis. The information gathered provides insight into the effect of increasing the number of multi-sensor data in land cover classification and the associated accuracies. Conventionally, many studies have relied on a single remote sensing data source, such as Landsat 8 or Sentinel-2. However, the fusing of multiple data sources has the potential to improve the temporal resolution of observations, due to different acquisition time from different sensors. For instance, (Hosseini et al. 2024) employed multi-source and temporal approach in mapping Cropping Intensity Patterns (CIPs), demonstrating the effectiveness of combining Sentinel-2 and Landsat 8/9 data. This synergy of multi-sensor enabled the generation of detailed phenological time series, which improved classification accuracy by effectively capturing the temporal dynamics of agricultural landscapes.

Likewise, stacking multi-sensor data from Synthetic Aperture Radar (SAR) and optical imagery harnesses the complementary strengths of both datasets. Optical images offer rich spectral information and clear visual details, but often diminished in quality particularly by cloud cover. In contrast, SAR data are largely unaffected by weather conditions, enabling consistent data. SAR imagery provides valuable texture features and surface roughness information, capturing the scattering characteristics of objects irrespective of environmental factors. By integrating SAR and optical data, it becomes possible to exploit their combined spatial, spectral, and scattering attributes, thereby enhancing target detection and improving the accuracy of LULC classification (Irfan et al. 2025).

Most existing literature on LULC mapping for the study area does not rely on previous or legacy maps to guide the generation of thematic land cover classes for comparative analysis. As a result, the LULC maps produced over the years are not directly comparable. Moreover, most studies focusing on this savanna landscape have used a single source of remote sensing data. This approach poses challenges in capturing certain patterns, as persistent cloud cover and the limited temporal resolution of the data often fail to resolve these issues, thereby affecting classification accuracy. Additionally, existing machine learning (ML) models struggle to effectively integrate multi-source remote sensing data, which can result in some patterns being poorly represented in the output. Finally, many of the gap-filling methods employed in current literature either shrink or expand the edges of gaps in classified images without adequately utilizing the spectral information from gap neighbouring pixels, thereby reducing the reliability of the information provided.

The main contributions of this article are as follows:

- Provision of 2023 annual LULC map based on the harmonization of previous LULC maps. The thematic land cover classes were aligned with legacy LULC
- Integration of multi-sensor remote sensing data. Composite of Synthetic Aperture Radar (SAR) and multispectral data with different temporal resolutions. The

approach capable of capturing land cover changes that otherwise would have been overlooked by individual sensors.

- Application of the Random Forest (RF) model for LULC classification. RF's ability
  to handle high-dimensional datasets and avoid overfitting makes it ideal for mapping savanna landscape dynamics as compared to Support Vector Machine (SVM).
- Applied gap-filling by incorporating information from neighbouring pixels.

The article is organized as follows: Section 2 describes the study area and dataset employed in the study, Section 3 outlines the classification methods employed, Section 4 presents the results, Section 5 discusses the research findings, and Section 6 concludes the study.

#### 2. Materials

#### 2.1. Study area

Agriculture is the main economic activity in the study area, with some commercial activities occurring in metropolitan cities and towns (Ferreira et al. 2022). It is situated in the northern part of Ghana and is comprised of five (5) regions (Figure 1). The area has savanna vegetation which is characterized by a mixture of grass and trees. The climatic condition is tropical with distinct wet and dry seasons, and it is

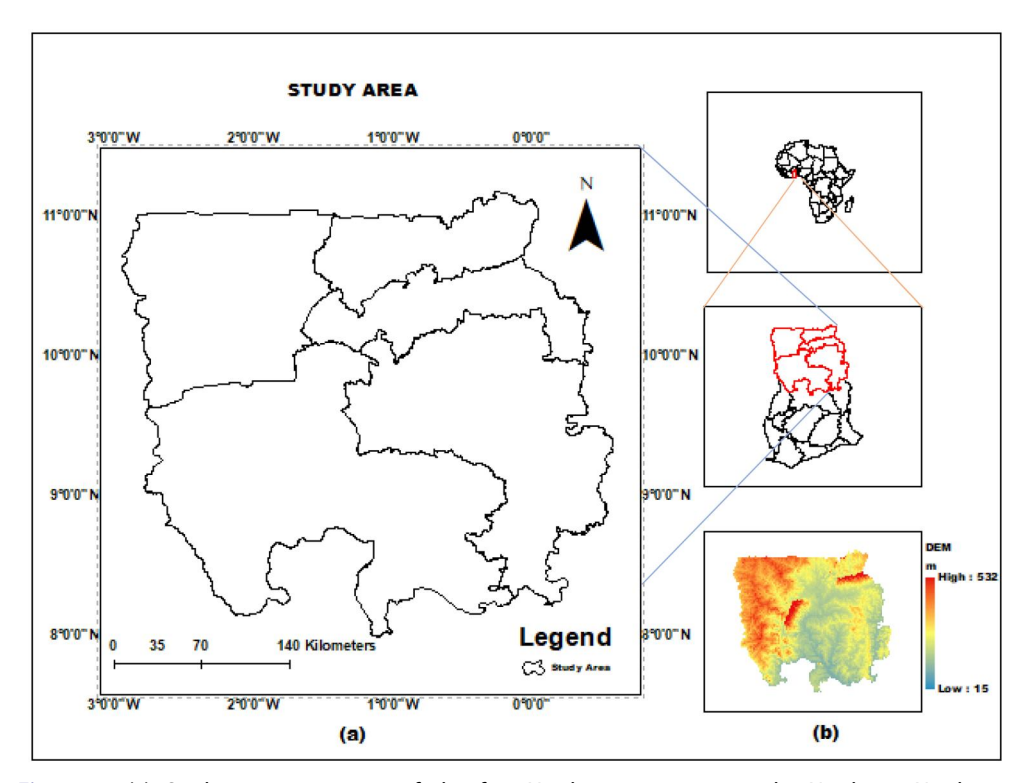


**Figure 1.** (a) Study area comprises of the five Northern regions, namely: Northern, Northeast, Savanna, Upper West and Upper East regions. (b) Digital elevation model (DEM) of the study area (values indicate areas with varying elevations above mean sea level).

slightly hotter and drier than the national average, with daily temperatures ranging from 30 to 40 °C and rainfall from 900 mm to 1200 mm.

#### 2.2. Dataset

Satellite imagery from Landsat 8, Sentinel-1, and Sentinel-2 products covering the period from January 1, 2023 to December 31, 2023 were used in this study (Table 1). Landsat 8 and Sentinel-2 provided multispectral data with spatial resolutions of 30 m and 10 m respectively. These multispectral datasets were complemented by Synthetic Aperture Radar (SAR) data from Sentinel-1, as radar imagery can deliver information on the land surface, even in situations of cloud cover. This is particularly relevant in the study area because cloud cover is frequent, particularly during the rainy season.

Table 1. List of satellite images used.

	•			
Product name	Spatial resolution	Temporal resolution	Period used	Origin
Landsat 8	30 m	16 days	01 to 12/2023	(Zhang et al., 2023)
Sentinel-1	10 m	6 days	01 to 12/2023	(Gargiulo et al., 2020)
Sentinel-2	10 m	5 days	01 to 12/2023	(Wang and Atkinson, 2018)
SRTM	30 m	_	-	(Farr et al., 2007)

The Landsat 8 Operational Land Imager/Thermal Infrared Sensor (OLI/TIRS) Collection 2 atmospherically corrected imagery at the Surface Reflectance (SR) level available in the Google Earth Engine (GEE) was used. A cloud cover filter of 30% per scene was applied, and cloud and cloud shadow values from the QA Pixel band of the Landsat data were used to masked the remaining clouds.

Sentinel-2 level-2 orthorectified atmospherically corrected surface reflectance images freely available in the Google Earth Engine (GEE) was used. A percentage of cloudy pixels was applied to select images with less than 20% cloud cover. Additional cloud pixel masking was applied by employing the quality assurance (QA) band of Sentinel-2. In addition, Sentinel-1 Ground Range Detected (GRD) images are also available in the Google Earth Engine (GEE), which has already been processed for calibration, and ortho-corrected products were used.

#### 3. Methods

#### 3.1. Harmonization of classification legend

For defining the thematic classes of the presented map, previous LULC maps of the study area from the year 2006 (Gessner et al. 2015) and 2015 (Forkuor et al. 2017) were harmonised due to their comparable legends and their class descriptions based on the Land Cover Classification System (LCCS) defined by FAO and UNEP as the reference classification system (Gregorio and Jansen 2000).

Through ten harmonized thematic classes, reference data for training and validation were collected during an intensive field campaign for three months between May and July 2023. For each field sample, coordinates in Geographic Coordinate

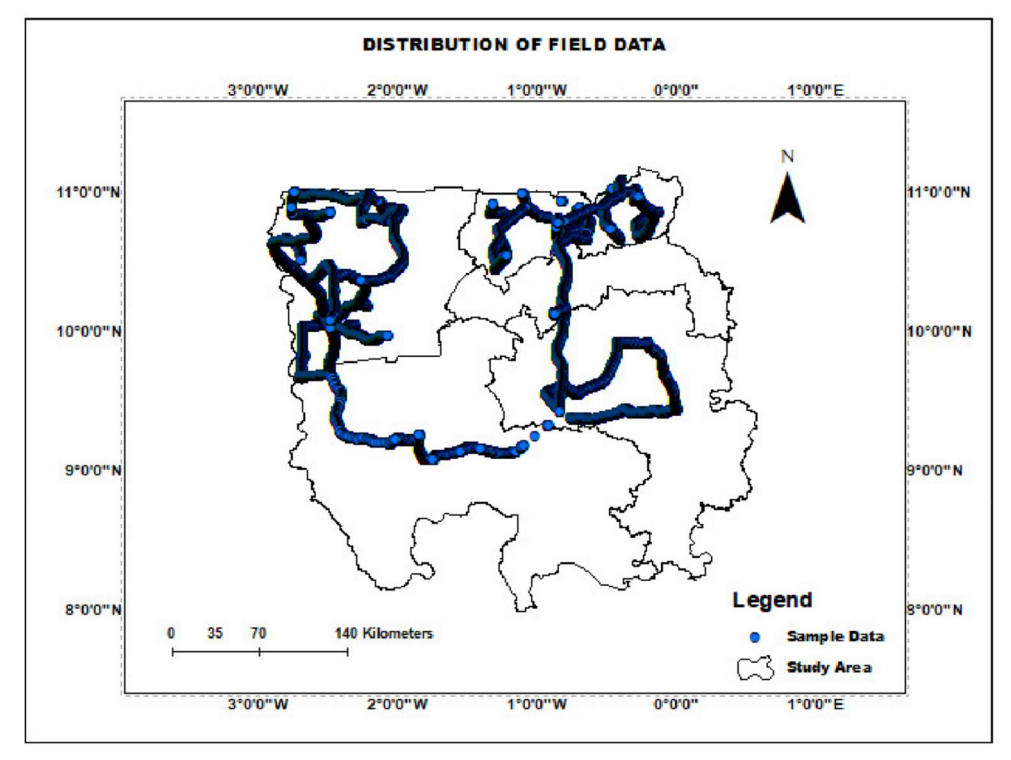


Figure 2. Distribution of field data collection in the study area.

System WGS 1984 (GCS\_WGS\_1984) were recorded using a Global Positioning System (GPS) device (Garmin GPSMAP 64s Handheld GPS Unit). Subsequently, the code for such thematic land cover class was assigned on the device and as well recorded in field notebook. These samples were collected along major roads, feeder roads, farm roads and accessible areas, as shown in Figure 2. Overall, the five northern regions of Ghana were covered, coincidentally covering the Sudan and Guinea savanna ecological zones, which are ecological zones severely impacted by climate change in Ghana.

#### 3.2. Satellite data processing

The remotely sensed data covering the entire study area with less cloud cover were processed to span the entire year in which the data were collected. All datasets that showed a cloud cover of more than 30% for Landsat 8 and 20% for Sentinel-2 were excluded from the complete archive of satellite imagery. The remaining cloud and cloud shadows on the images were masked by applying a quality assurance (QA\_Pixel) band associated with Landsat 8. Similar masking was performed by employing the quality assurance (QA60) band of Sentinel-2.

Landsat 8 and Sentinel -2 as well as Landsat 8, Sentinel -2 and Sentinel -1 images were stacked and used as the two primary input data as shown in Figure 3 Data stacking. This approach harnesses the capabilities of two multispectral images

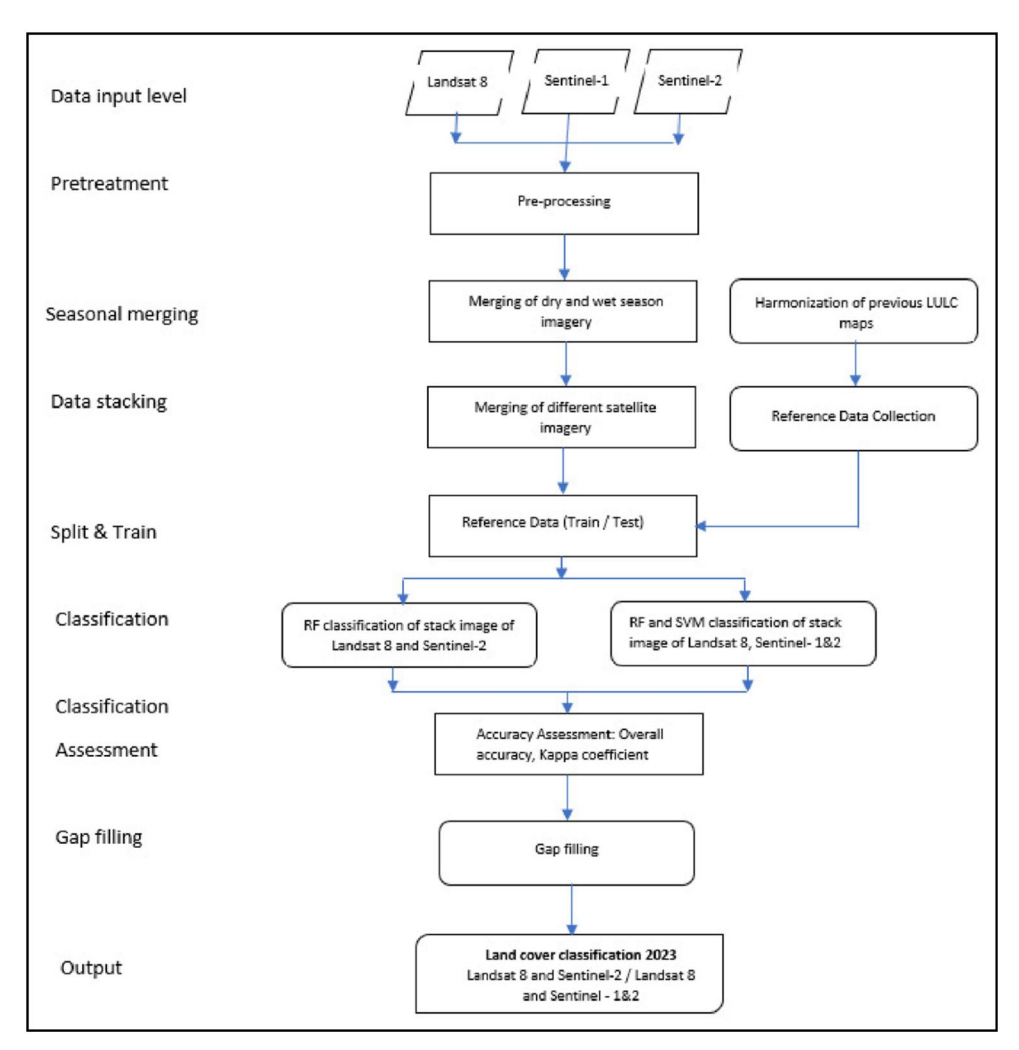


Figure 3. Workflow.

and then a combined optical and radar images to map the tropical savanna landscape. Subsequently, several indices were computed for both the optical and radar satellite imagery. This was done to enhance the spectral variability between bands and reduce the topographic effect. The selected indices, have shown the potential to provide vital information for the intended land cover classification assessment.

The Normalized Difference Vegetation Index (NDVI) is correlated with vegetation greenness, density, and productivity (Sobrino et al. 2004).

Thus:

$$NDVI = \frac{NIR - Red}{NIR + Red}$$
 (1)

where NIR is the reflectance in the near-infrared band, and Red is the reflectance in the red band.

To enhance separability of land from aquatic vegetation, the Normalized Difference Aquatic Vegetation Index (NDAVI) was employed (Villa et al. 2014).

$$NDAVI = \frac{NIR - Blue}{NIR + Blue}$$
 (2)

where NIR is the reflectance in the near-infrared band, and Blue is the reflectance in the blue band.

To enhance water features, extract water information of an area, and reduce noise from anthropogenic features and vegetation, the Modified Normalized Difference Water Index (MNDWI) was estimated (Xu 2006).

$$MNDWI = \frac{Green - SWIR1}{Green + SWIR1}$$
 (3)

where Green is the reflectance in the green band and SWIR1 is the reflectance in the shortwave infrared 1 band.

To continue with spectral variability enhancement among bands, band ratios were employed to enhance the appearance of features in the image (Ghrefat et al. 2023). They distinguish the minor characteristics of features that are otherwise masked as a result of spectral variations. Therefore, the band ratio is good at amplifying features being analyzed by rescaling or stretching the result, which are then shown as new images (Shahi et al. 2023). Three band ratios, Simple Ratio (RS), Band Ratio 6/5 (ratio65) and Band Ratio 4/6 (ratio46) were computed to enhance the spectral variability of the image used (Table 2).

Table 2. Band ratio indices.

Ratio	Formula	Comments
Simple ratio	$SR = \frac{NIR}{Red}$	Where NIR is reflectance in the near infrared band and Red is reflectance in the red band (Kior et al., 2021).
Band ratio 6/5	$ratio65 = \frac{SWIR1}{NIR}$	Where SWIR 1 reflectance in the shortwave infrared 1 band and NIR is reflectance in the near infrared band (Olasunkanmi et al., 2023)
Band ratio 4/6	$ratio46 = \frac{Red}{SWIR1}$	Where Red is reflectance in the red band and SWIR is reflectance in the shortwave infrared band 1 (Seleim et al., 2022)

To estimate chlorophyll content of the vegetation cover Green Chlorophyll Vegetation Index (GCVI) was employed to compute the reflectance image (Wu et al. 2012).

$$GCVI = \left(\frac{NIR}{Green}\right) - 1 \tag{4}$$

where NIR is the reflectance in the near-infrared band, and Green is the reflectance in the green band.

For soil adjusted vegetation index (SAVI) seeks to lessen the impact of soil intensity by employing soil-brightness correction factor (Huete 1988).

$$SAVI = \left(\frac{(NIR - Red)}{(NIR + Red + 0.5)}\right) * 1.5$$
 (5)

where NIR is the reflectance in the near-infrared band, and Red is the reflectance in the red band.

For Synthetic Aperture Radar (SAR) imagery, the Radar Vegetation Index (RVI) (Sahadevan et al. 2013) was estimated to provide a comprehensive level of vegetation growth in areas hindered by dense cloud cover.

$$RVI = \frac{4\sigma^{0}_{HV}}{\sigma^{0}_{HH} + \sigma^{0}_{VH}}$$
 (6)

where  $\sigma$ HH is the polarised backscattering coefficients and  $\sigma$ HV is cross polarization coefficients.

The Radar Forest Degradation Index (RFDI) (Joshi et al. 2015) estimate.

$$RFDI = \frac{n\sigma^{0}_{HH} - n\sigma^{0}_{HV}}{n\sigma^{0}_{HH} + n\sigma^{0}_{HV}}$$
 (7)

where  $\sigma$ HH is the polarised backscattering coefficients and  $\sigma$ HV is cross polarization coefficients.

These indices and masking were applied to images on a seasonal basis. Thus, processing was performed for all Landsat 8 images in the wet and dry seasons. Then, the images were merged to correspond to the study year. This procedure was subsequently repeated for Sentinel-1 and Sentinel-2 respectively.

#### 3.3. Random forest and support vector machine classification

The random forest ensemble model applies the bagging technique, where each tree is built or grown independently by bootstrapping (generating) a dataset sample with replacement from an existing dataset and output, which is the aggregation of each tree (Breiman 2001; Belgiu and Dragut 2016; Umoh et al. 2022; Islam et al. 2023). The dataset for the trees was randomly chosen. Randomness is introduced during the training phase in two approaches, in sub-sampling the training data, each tree is grown using a different subset, and in node test selection (Boateng et al. 2020). RF is a nonparametric model, meaning it does not assume any fixed functional form and that the shape of the data is learned from the data itself. This makes RF produce more accurate results and therefore, has considerable advantages over other models. (Lu et al. 2012; Sonawane and Dhawale 2016). Good performance of the model was achieved with a sufficient number of defined trees and a relevant number of predictors available. An ideal way to determine if the number of trees is sufficient is to compare whether the prediction made by the subset of the forest works well with that of full forest prediction (Boateng et al. 2020). The target of SVM is to detect an optimal hyperplane that assigns a data into distinct classes. This is enabled by a kernel function that takes input feature into a higher-dimensional space (Hosseini et al. 2024). As a non-parametric model, SVM does not make assumptions about the underlying data distribution, therefore being robust to variations in data characteristics (Mountrakis et al. 2011).

RF and SVM were employed in this study, with approximately 75% of the sample dataset used as the training set and 25% for testing the developed model. Two classification processes were setup, the first was the multispectral image stack of Landsat 8 and Sentinel-2. Preceding the stacking, the Sentinel-2 bands were renamed to correspond to those of Landsat 8, and subsequently, its resolution was converted to that of Landsat. The other image stack consisted of both optical images of Landsat 8 and Sentinel-2 and radar image of Sentinel-1. The Sentinel-1 resolution was converted to a 30 m resolution of Landsat 8. Other pre-processing involved normalization of radar backscatter using reference incident angle and reducing variability across acquisition time by performing temporal normalization was carried out.

Based on the harmonization process, the ten thematic classes were deduced and samples were taken from the field campaign to perform the classification process. It was established that there were similarities in the classes, mainly in the vegetation classes. This informed the merging of classes with similarities to improve the classification accuracy. Finally, image classification was performed by employing six distinctively land cover thematic classes namely: Cropland, Water, Town, Vegetation, Bareland, and Grass as the training set samples to classify the image.

The classification was validated to determine the accuracy of the results (Figure 3). This was performed using the remaining data that was split. The classification accuracy was assessed by comparing the predicted and actual variables. Accuracy assessment was performed using overall accuracy (OA), kappa coefficient index, omission, commission, producer accuracy, user accuracy, and F1-score (F1), as this is the current standard to evaluate classification accuracies in many Earth Observation (EO) research studies (Stumberg et al. 2014; Tallón-Ballesteros and Riquelme 2014; Shivakumar and Rajashekararadhya 2018; Shawky et al. 2019).

The overall accuracy of the confusion matrix (Shivakumar and Rajashekararadhya 2018).

Overall Accuracy = 
$$\frac{N \sum_{i=1}^{m} \text{Dii}}{N}$$
 (8)

where Dii is the diagonal pixels of class i and N is the total number of pixels in the confusion matrix.

Cohen's kappa for the confusion matrix was based on (Tallón-Ballesteros and Riquelme 2014).

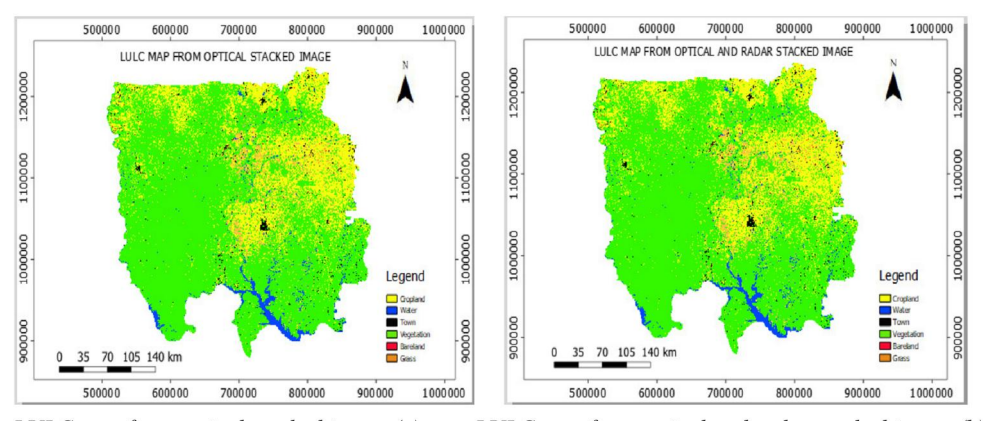
Cohen's Kappa = 
$$\frac{N \sum_{i=1}^{m} DM - \sum_{i=1}^{m} Er * Ec}{N^2 - \sum_{i=1}^{m} Er * Ec}$$
(9)

where N is the total number of pixels. DM represent the diagonal pixels (elements) of the confusion matrix, Er is the total number of pixels in row i, Ec is the total number of pixels in column i, and m is the number of rows.

The classification results had some gaps caused by excessive cloud cover, leading to missing data and making interpretation in these gap spots severely restricted (Wang et al. 2022). Existing spatial gap-filling methods often imply gap edge expansion or shrinkage. This means that, spatial gap-filling approaches need to estimate the missing pixel value from the surrounding pixels rather than further pixels (Mohammed 2013; Yan and Roy 2018). Here, a majority filter was applied, which made use of the information from the defined neighbourhood (moving window) to fill the gaps by ensuring that the value given to the gaps was representative of the nearby pixels (Habib et al. 2004). An interactive approach was adopted, and the kernel size was defined in such a way that all gaps were identified and filled accordingly. Furthermore, the area covered by each class and percentage of area coverage were computed.

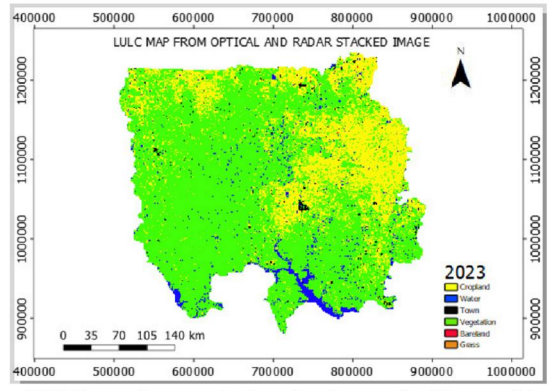
#### 4. Results

Land Use Land Cover at disturbed and undisturbed locations in the Sudan and Guinea ecological zones in Ghana with six land use classes were analyzed. The results presented in Figure 4 provide a highly accurate land cover map of 2023 produced



LULC map from optical stacked image (a)

LULC map from optical and radar stacked image (b)



LULC map from optical and radar stacked image (b)

Figure 4. LULC map of 2023, (a) and (b) produced by RF, (c) produced by SVM.

from the stacked images of Landsat 8, Sentinel 1 and Sentinel 2 at 30 m resolution. The land use classes presented in the map are based on the harmonised legend derived from the previous map of 2006 and 2015 which were consistent with the Land Cover Classification System (LCCS) defined by the FAO and UNEP as the reference classification system (Gregorio and Jansen 2000). The Random forest classification approach was very efficient as it was able to capture land uses in the savanna landscape (study area) with an overall accuracy of 73.32% and a Kappa coefficient of 0.6342 for a stacked image from optical data of Landsat 8 and Sentinel-2 and for a stacked image from both optical and radar images (Landsat 8, Sentinel 1, and Sentinel 2) achieved an overall accuracy of 80.21% and a Kappa coefficient of 0.7225, indicating an improve performance of 6.89%. However, when Support Vector Machine (SVM) was used, the model achieved an overall accuracy of 77.38% and a Kappa coefficient of 0.6651 for stacked composite of optical and SAR images. This demonstrated a better performance of RF over SVM of 2.83% in the study area.

The matrix in Table 3 consists of rows and columns of classes (pixels) depicted in the map as a result of the classification of the stacked image and classes represented in the reference data. The resultant diagonal cells provide information about correctly classified cells, whereas other cells represent errors of commission and omission (Freitas et al. 2024). To extract the information captured in the confusion matrix, several formulas were deduced and estimated, including overall accuracy (OA), kappa coefficient index, error of omission, error of commission, producer accuracy, user accuracy and F1-score (F). OA gives the proportion of correctly classified pixels (cells) from the total number of pixels (cells). This provides degree of general model accuracy across all classes combined (Figure 5). The kappa coefficient on the other hand, determines how well the classification results agree with the true labels. It provides a more robust metric than OA.

The gap filling measure adopted makes use of the spatial filling technique by inspecting neighbouring pixels of a gap and replacing it with the most frequent value among its neighbours. Because it is useful for categorical data, the results of the majority filter applied to the classified image are shown in Figure 6, as all the gaps in the image were effectively identified and filled with respect to their neighbouring pixel values accordingly.

The extracted land use area of coverage was subsequently estimated using the percentage they occupied, as presented in Table 4. In addition, regional land use area coverage as well as the percentage they constitute were analyzed as presented in Figures 7 and 8 below. The findings showed that, the Northern region constitutes 39.15% of the cropland area in the study area. In addition, the Savanna region accounts for 71% and 46.81% of the water and vegetation coverage respectively, in the research area.

#### 5. Discussion

The study employed the Random Forest (RF) and Support Vector Machine (SVM) algorithms with stacked satellite images (Landsat 8, Sentinel-1 and Sentinel-2) to map the spatial distribution of land cover classes for the year 2023. The high classification

Table 3. Cross tabulation between reference data and classified data of 2023 with six (6) land use classes, namely: cropland, water, town, vegetation, bareland and grass. (A) Cross-tabulation of stacked optical data classification

				Referen	Reference data						
		-	:	ı	;	-	,		Error of	Producer	i
		Cropland	Water	Town	Vegetation	Bareland	Grass	Total	commission	accuracy	F1-score
Classified data	Cropland	69	-	8	13	0	0	91	0.2418	0.7582	0.6667
	Water	5	36	٣	14	0	0	28	0.3793	0.6207	0.7501
	Town	13	0	42	5	0	-	61	0.3115	0.6885	0.6999
	Vegetation	21	0	-	148	_	4	175	0.1543	0.8457	0.8109
	Bareland	7	-	4	4	12	0	28	0.5714	0.4286	0.5715
	Grass	_	0	_	9	_	6	18	0.5	0.5	0.5626
	Total	116	38	59	190	14	14	431			
	Error of ommosion	0.4052	0.05263	0.2881	0.221	0.1429	0.3571				
	User accuracy	0.5948	0.9474	0.7119	0.7789	0.8571	0.6429				

(B) Cross-tabulati	) Cross-tabulation of combined optical and		radar data classification from RF	n RF							
				Refere	Reference data						
		Cronland	Water	Town	Vegetation	Bareland	Grace	Total	Error of	Producer	F1-score
Classified data	Cropland	02	2	-	7	0	G C	80	0.1250	0.8750	0 7407
	Water	2 9	32	- 0	1	0	0	49	0.3469	0.6531	0.7711
	Town	9	0	40	-	0	0	47	0.1489	0.8511	0.8889
	Vegetation	18	0	<del>-</del>	146	-	m	169	0.1361	0.8639	0.8513
	Bareland	8	0	-	3	11	0	23	0.5217	0.4783	0.6287
	Grass	_	0	0	9	0	6	16	0.4375	0.5625	0.6429
	Total	109	34	43	174	12	12	384			
	Error of ommosion	0.3580	0.0588	0.0700	0.1609	0.0833	0.2500				
	User accuracy	0.6422	0.9412	0.9302	0.8391	0.9167	0.7500				

(C) Cross-tabulation of combined optical and radar data from classification from SVM

				Reference data	ce data						
		Cropland	Water	Town	Vegetation	Bareland	Grass	Total	Error of commission	Producer accuracy	F1-score
Classified data	Cropland	47	-	0	14	0	0	62	0.2419	0.7581	0.6714
	Water	2	33	0	10	0	0	48	0.3125	0.6875	0.7857
	Town	9	0	29	<b>-</b>	0	0	36	0.1944	0.8056	0.8923
	Vegetation	14	2	0	125	0	0	141	0.1135	0.8865	0.8306
	Bareland	3	0	0	9	-	0	10	6.0	0.1000	0.1818
	Grass	3	0	0	4	0	-	80	0.8750	0.1250	0.2222
	Total	78	36	29	160	-	-	305			
	Error of ommosion	0.3974	0.0833	0.0000	0.2188	0	0				
	User accuracy	0.6026	0.9167	1.0000	0.7813	1	_				

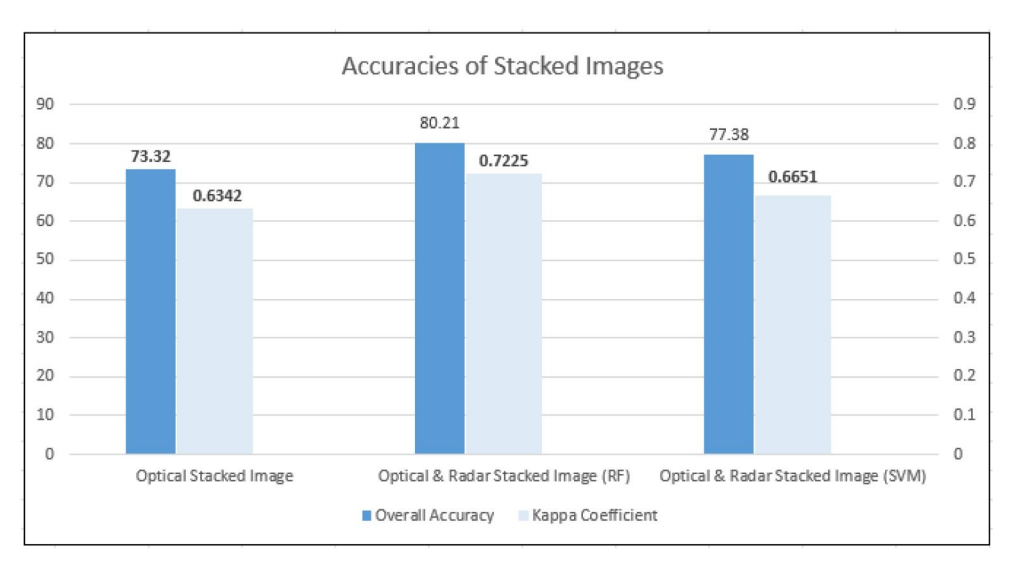
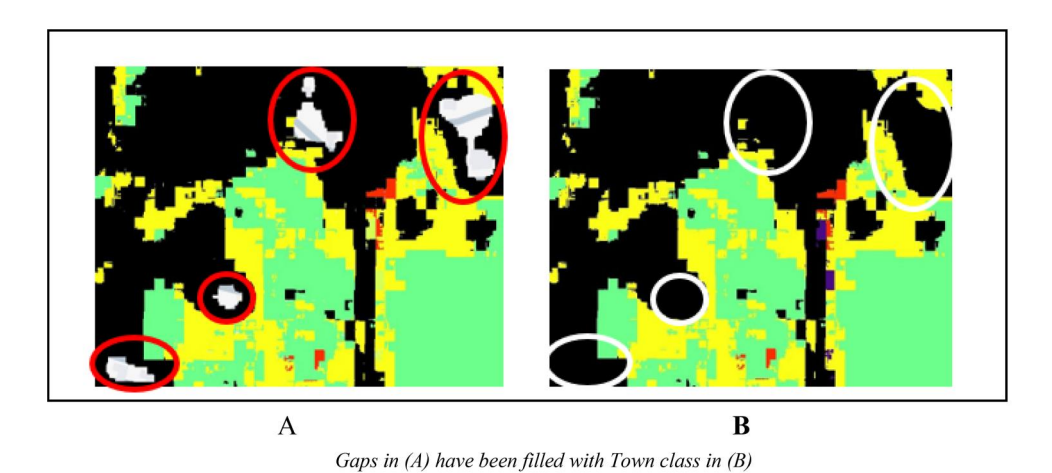
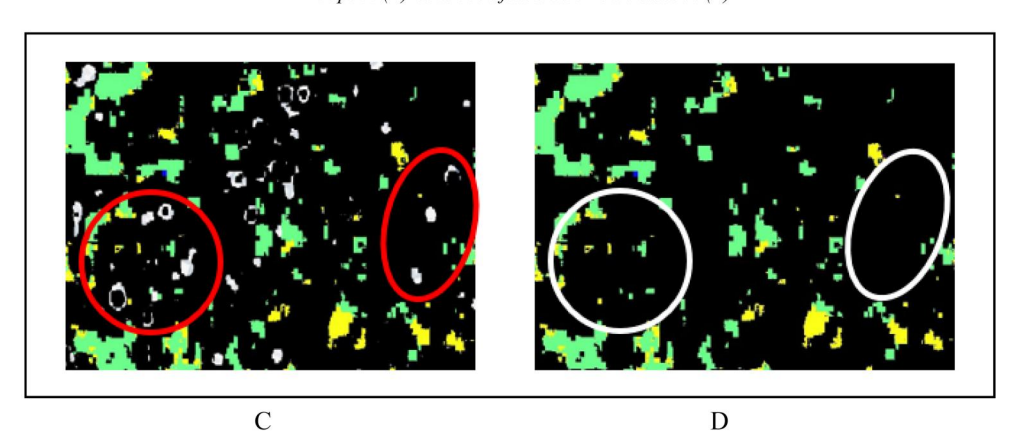


Figure 5. Comparison of accuracies of both optical stacked and combined radar and optical images.





White gaps in (C) have been filled with town class in (D)

Figure 6. Gap filling in a classified image.

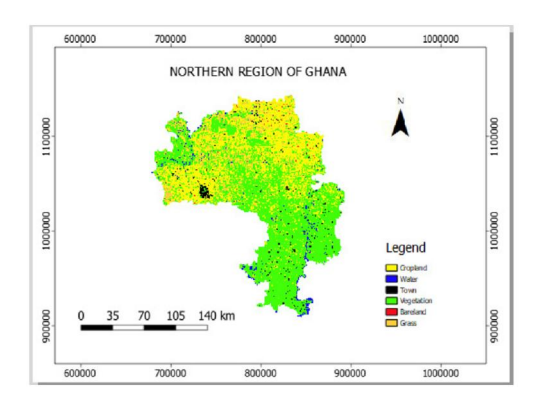
Table 4. Alea alla	percentage coverage or thematic classes.	
Class name	Area (Sq.Km)	Area (%)
Cropland	22502.8023	23.3847
Water	2426.0096	2.5210
Town	1138.7204	1.1833
Vegetation	66975.2771	69.6002
Bareland	144.4678	0.1501
Grass	3041.1941	3.1603
Total	96228.4713	100

Table 4 Area and percentage coverage of thematic classes

accuracy of 80.21% and 77.38% and kappa coefficient of 0.7225 and 0.665 for RF and SVM respectively are an indication of RF efficiency in mapping heterogeneous landscapes using multi-sensor imagery (Figure 5). The results were in tune with (Adugna et al. 2022), who found that Random Forest (RF) out performed Support Vector Machine (SVM) in a classification process to create Land Cover map. It states that, RF performed well in a mixed class classification and also able to handle efficiently large dataset input where SVM founds it challenging. It therefore an indicative that RF is robust for heterogeneous landscape mapping.

Also, the Random Forest classification results obtained were consistent with those of studies conducted in the region such as (Gessner et al. 2015) who employed RF in multi-sensor mapping of West African land cover using MODIS, ASAR, and TanDEM-X/TerraSAR-X data with an accuracy of 80% at legend level 1 (9 classes) and 73% at legend level 2 (14 classes). Kappa coefficients calculated were 0.77 at level 1 and 0.71 at level 2 respectively. The findings were as well consistent with (Zoungrana and Dimobé 2023), who predicted the vegetation trend classes in the Sudanian savanna with an overall accuracy and kappa value of 82% and 0.76, respectively. Equally, the predictive performance of RF was observed by Yangouliba et al. (2022) who used RF to model LULC for 1990, 2005, and 2020 and had an overall accuracy of 81%, 91%, and 93% and kappa coefficients of 0.91, 0.82 and 0.76, respectively.

The ability to distinguish other land use classes from the scene implies the capacity of the fused imagery to be used as primary data for mapping heterogeneous savanna landscapes. Other studies such as (Ibrahim 2023) have employed a Random Forest (RF) based feature selection approach using Sentinel-1, Sentinel-2, and Shuttle Radar Topographic Mission (SRTM) data. The results indicated that Sentinel-2 data only achieved an overall accuracy of 84.2%, while Sentinel-1 and SRTM data achieved 83% and 76.44%, respectively. The classification accuracy improved to 89.1% when Sentinel-2, Sentinel-1, and SRTM data were combined. This represents a 4.9% improvement in overall accuracy compared to Sentinel-2 alone and a 6.1% and 12.66% improvement compared to Sentinel-1 and SRTM data respectively. Again, (Pastick et al. 2020) employed a harmonized Landsat 8 and sentinel-2 to mapping of invasive annual grass with a high overall accuracy of above 81%. (Onačillová et al. 2022) combined Landsat 8 and Sentinel-2 data from Google Earth Engine to derive high resolution Land Surface Temperature maps in urban environments with an accuracy within acceptable limits.



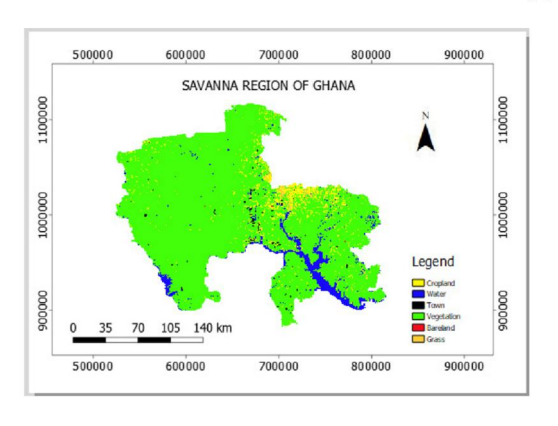
	Northern Regio	n
Class	Area (Sq.Km)	Area (%)
Name		
Cropland	8808.7731	35.8271
Water	408.515	1.6615
Town	445.3929	1.8115
Vegetation	13346.8698	54.2845
Bareland	57.1483	0.2324
Grass	1520.1842	6.1829
Total	24586.8833	100

700000 800000 NORTH EAST REGION OF GHANA 80 km

800000

700000

N	orth East Regio	n
Class	Area	Area (%)
Name	(Sq.Km)	
Cropland	4062.7863	44.9740
Water	117.0232	1.2954
Town	174.2284	1.9286
Vegetation	3888.9782	43.0500
Bareland	16.9166	0.1872
Grass	773.6904	8.5645
Total	9033.6231	100



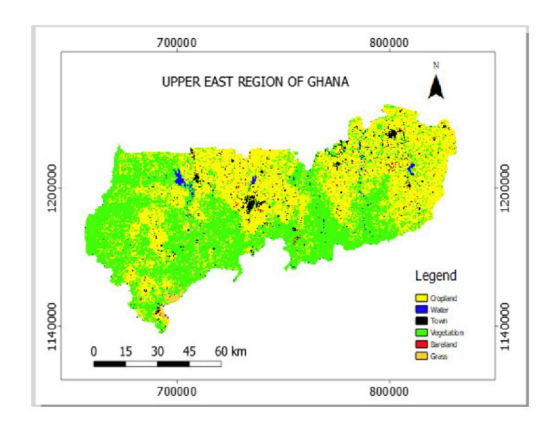
	Savanna Region	
Class	Area	Area (%)
Name	(Sq.Km)	
Cropland	1653.4094	4.6488
Water	1722.3837	4.8427
Town	161.9353	0.4553
Vegetation	31607.5137	88.8700
Bareland	3.9878	0.0112
Grass	416.76	1.1717
Total	35565.9899	100

Figure 7. Regional land use analysis in the study area (a-e).

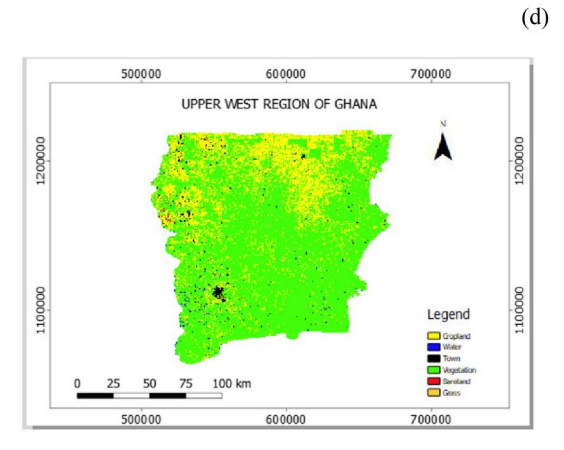
The study also examined the results when optical and radar images were fused as input data for LULC classification using the RF algorithm in GEE. The results showed that adding radar image Sentinel-1 along with Landsat 8 and Sentinel-2 images in the GEE improved the image classification accuracy. This finding is

(a)

(b)



Uı	pper East Region	1
Class Name	Area	Area (%)
	(Sq.Km)	85 86
Cropland	3879.2107	45.4735
Water	93.9726	1.1015
Town	177.5774	2.0816
Vegetation	4180.2699	49.0026
Bareland	36.6309	0.4294
Grass	163.0351	1.9111
Total	8530.6966	100



U	pper West Regi	on
Class	Area	Area (%)
Name	(Sq.Km)	
Cropland	4106.1046	22.1122
Water	97.4211	0.5246
Town	180.0317	0.9695
Vegetation	13986.7315	75.3214
Bareland	29.851	0.1607
Grass	169.2366	0.9113
Total	18569.3765	100

Figure 7. Continued.

(e)

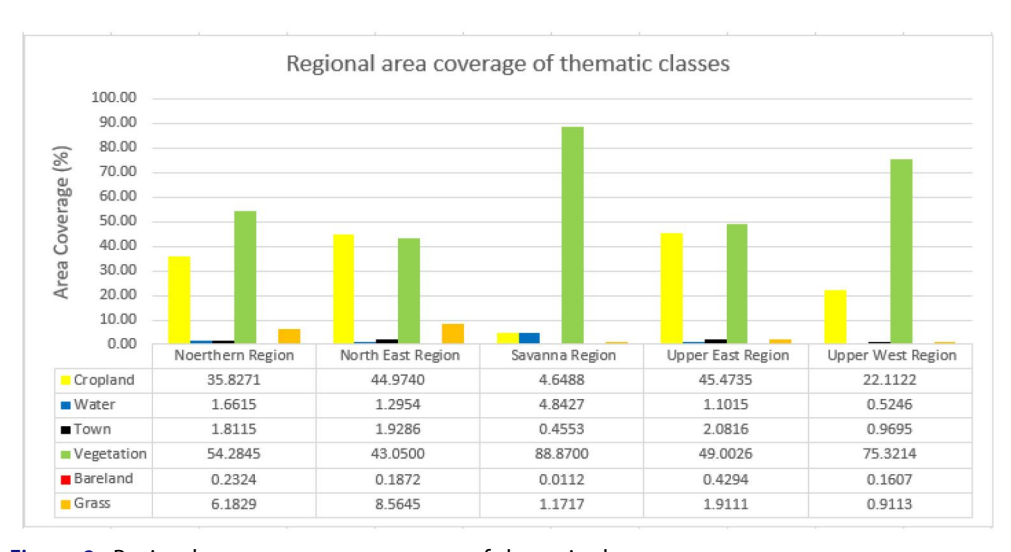


Figure 8. Regional area percentage coverage of thematic classes.

consistent with other studies (Lee et al. 2024), which used a combination of Korean Multi-purpose Satellite 3 (KOMPSAT-3), KOMPSAT-5 SAR, Compact Advanced Satellite 500-1 (CAS500-1), Sentinel-1, and Sentinel-2 within GEE as well as NDVI from CAS500-1 and KOMPSAT-3 and confirmed that a continued improvement in classification accuracy occurred as the number of satellite images applied as input data increased. Therefore, we emphasize the use of multi-sensor data to improve classification results. The accuracy of the LULC classification was also in line with a study by Nhemaphuki et al. (2020). who produced LULC maps using optical and radar data and a combination of both by employing the Random Forest algorithm. The results indicated that the fusion of optical and radar data gave better land cover discrimination with 96.98% overall accuracy in comparison to using radar and optical data separately, with overall accuracies of 69.2% and 95.89% respectively.

The classification process in this study involved the use of a stacked image derived from multi-sensor satellite data, specifically Landsat 8, Sentinel-1, and Sentinel-2. While the integration of multiple sensors enhances the quality of information available for land cover classification, combining spectral, spatial, and backscatter data, involves high computational cost associated with processing such stacked datasets. This increased computational demand, which was one of the constraints of the study, was as a result of the sheer volume of data involved and the complexity of harmonizing images with varying spectral characteristics and temporal acquisition periods (Fang et al. 2023).

Although the classification accuracy achieved using a stacked multi-sensor image comprising Landsat 8, Sentinel-1, and Sentinel-2 was relatively high, there remains considerable potential for improvement if the spatial resolution of the composite had been finer. In the present study, the image stack integrated data at the coarser 30 m resolution of Landsat 8, rather than harmonizing to the finer 10 m resolution of Sentinel-2. This is because spatial resolution plays a crucial role in land cover classification performance, especially in heterogeneous landscapes such as the savanna zones of the study area, where small-scale land cover features could easily be aggregated into dominant land cover at coarser resolutions (Tassi et al. 2021).

Stacked composites derived from SAR and optical data such as those from Landsat 8, Sentinel-1, and Sentinel-2 offer improved spectral and temporal diversity (Inglada et al. 2016). Leveraging these multi-sensor datasets improved class discrimination by combining spectral reflectance, backscatter, and texture information. However, in this study, such stacking increases the dimensionality of the dataset, potentially introducing redundant or noisy features. While the Random Forest (RF) algorithm, particularly through parameters used (Number of Trees: 300 and Variable Per Split: 6), can hand high-dimensional data to some extent, its performance is influence by how these parameters are set. (Rodriguez-Galiano et al. 2012).

The selection of an appropriate gap-filling method is largely determined by the specific application and data characteristics. In the present study, one of the key challenges was filling gaps in the imagery caused by cloud cover. A majority filter was employed to address this issue, achieving a reasonable degree of accuracy in reconstructing the missing areas. However, more advanced approaches could improve the accuracy achieved. For instance, (Aliabad et al. 2024) applied Multi-channel Singular Spectrum Analysis (MSSA) to reconstruct MODIS land surface temperature (LST) imagery, achieving notably high accuracy in gap-filling. Their findings indicated that, MSSA approach reconstructed MODIS–LST image with root mean square error (RMSE) of 2.6 °C for the entire study region and 1.4 °C for a selected pixel. These results demonstrate MSSA ability to produce gap-free LST time series datasets. Similarly, (Malamiri et al. 2020) applied MSSA to also reconstruct Landsat derived normalized difference vegetation index (NDVI) images and confirmed the method's effectiveness for tackling missing-data in vegetation time-series analysis.

He et al. (2023) introduced the learnable correlation sub-pixel mapping network (LECOS), which employs a hierarchical self-attention mechanism to learn and visualize both sub-pixel spatial structure and pixel-level contextual relationships. This approach demonstrated the capability to substantially reconstruct very-fine urban LULC at 2 m resolution from Sentinel-2 imagery. Integrating LECOS into a multisensor workflow that combines optical and SAR data within a RF classification like in the present study could further enhance LULC mapping by resolving mixed pixels into their constituent land cover classes. Such an approach would be valuable for heterogeneous savanna landscapes, where conventional pixel level methods often struggle to capture fine-scale spatial heterogeneity. In a related advancement, (He et al. 2025) proposed the visual-language reasoning segmentation (LARSE) framework for function-level building footprint extraction. This hierarchical method combines visual context embedding with semantic reasoning, leveraging high-resolution imagery in conjunction with language-guided segmentation to identify and categorize building footprints by function. By integrating visual language models with segmentation techniques, LARSE offers robust capabilities for semantic LULC classification. The integration of LECOS with multi-sensor LULC data and LARSE within a unified workflow could deliver both the high spatial precision required for accurate classification and the semantic richness needed for functional interpretation, thereby surpassing the capabilities of traditional LULC mapping approaches.

The decision to merge similar land cover thematic classes in this study was primarily motivated by the need to reduce classification errors. This strategy has been shown to improve performance metrics such as overall accuracy and the kappa coefficient (Foody 2002). However, while such aggregation can enhance classification outputs, it inevitably reduces the ecological and biophysical resolution of the dataset. This loss of thematic detail can have significant implications for downstream applications, including biodiversity monitoring and carbon accounting. From a biodiversity perspective, merging classes with similar spectral or structural characteristics such as the consolidation of vegetation types undertaken in the present analysis diminishes ecological resolution as many species exhibit fine-scale habitat preferences (Jansen et al. 2005). Regarding carbon accounting, thematic aggregation can obscure substantial differences in aboveground biomass and soil carbon stocks, as similar vegetation types may vary prominently in carbon density due to differences in structural attributes, age, and distribution (Houghton and Hackler 2006). Therefore, merging thematically similar classes can improve accuracy of classification outputs (Congalton and Green 2008). However, the risk of reducing the utility of LULC products for applications that require high thematic specificity is real. The trade-off is that decisions on class merging should therefore be application-driven, and ideally, multi-scale products should be maintained to serve both coarse and fine-resolution needs.

Based on the demonstrated robustness of the multi-sensor data and Random Forest (RF) approach in classifying the savanna landscape in this study, the proposed workflow could be applied to other years to assess its effectiveness in detecting land cover changes, particularly interannual variations in vegetation phenology and climate. This framework also holds potential for application in other savanna or forested regions worldwide for landscape analysis. For example, (Fang et al. 2023) employed a similar multi-sensor approach integrating Sentinel-1, Sentinel-2, and Landsat-8 data using Random Forest and XGBoost models to extract forest variables. Likewise, (Lee et al. 2024) emphasized the importance of increasing the number of satellite datasets in multi-sensor approaches to enhance classification performance.

#### 6. Conclusions

In conclusion, this study focused on combining optical and radar data in land cover mapping using Random Forest and Support Vector Machine in GEE and examined the accuracies of LULC maps produced by combined optical sensors alone and both Optical and Radar sensors. The results confirmed that, adding the Sentinel-1 image to the already stacked optical images of Landsat 8 and Sentinel-2 significantly improved the accuracy of LULC classification. The high overall accuracy of the classification confirmed the suitability of the Random Forest approach for savanna landscape analysis for both small-and large-scale monitoring of land use changes.

The gap-filling method employed confirmed the effectiveness of using a defined neighbourhood window in searching for neighbouring pixel values to fill the gap. The majority filter proved to be the ideal, as it did not cause the gap edges to either shrink or expand. This approach is useful in study areas where there are gaps in data caused by excessive cloud cover.

The study utilized six land-cover classes derived from the harmonization of previous LULC maps for 2006 and 2015. Further research is recommended to subdivide the land cover classes to establish the dynamics of the classes at a higher class level and employ other machine learning algorithms to ascertain their performance. Therefore, a detailed classification can lead to the refinement in some of the classes, thereby enhancing the subsequent LULC outputs and increasing their value for downstream applications that require fine-scale resolution for monitoring purposes. Also, the thematic class estimations, have contributed to the understanding of their percentage coverage and will help in their future prediction in a comparative regional analysis.

#### **Author contributions**

Conceptualization, K.A., U.G., and A.B.O.; methodology, K.A.; validation, U.G. and A.B.O.; formal analysis, K.A.; investigation, K.A.; resources, F.D. and F.T.; data curation, K.A.; writing-original draft preparation, K.A.; writing-review and editing, K.A., F.D., F.T., U.G., and A.B.O.; visualization, K.A.; supervision, U.G. and A.B.O; project administration, F.D. and F.T.; funding acquisition, F.D. and F.T.

#### **Disclosure statement**

No potential conflict of interest was reported by the authors.

#### **Funding**

This research was funded by the German Federal Ministry of Education and Research (BMBF), and the funds were delivered to UNU-INRA through the West African Science Service Centre on Climate Change and Adapted Land Use (WASCAL) with grant reference number 01LG2101A.

#### Data availability statement

The land use thematic class data collected from the field and used to support the findings of this study may be released upon request from the United Nations University Institute for Natural Resources in Africa (UNU-INRA). The Landsat 8, Sentinel-1, and Sentinel-2 images are available on Google Earth Engine upon request.

#### References

- Adugna T, Xu W, Fan J. 2022. Comparison of random forest and support vector machine classifiers for regional land cover mapping using coarse resolution FY-3C images. Remote Sens (Basel). 14(3):574. doi:10.3390/rs14030574.
- Aliabad FA, Zare M, Malamiri HG, Pouriyeh A, Shahabi H, Ghaderpour E, Mazzanti P. 2024. Reconstructing daytime and nighttime MODIS land surface temperature in desert areas using multi-channel singular spectrum analysis. Ecol Inf. 83:102830. doi:10.1016/j.ecoinf. 2024.102830.
- Antwi EK, Kwabena Antwi E, Boakye-Danquah J, Boahen Asabere S, Yiran GAB, Loh SK, Gyekye Awere K, Abagale FK, Asubonteng KO, Attua EM, et al. 2014. Land use and land-scape structural changes in the ecoregions of Ghana. J Disaster Res. 9(4):452–467. doi:10. 20965/jdr.2014.p0452.
- Baade J, Le Roux JJ, Morgenthal T, Nghiyalwa HS. 2021 Apr 30. Land degradation in savanna environments assessments, dynamics and implications. EGU General Assembly 2021.
- Belgiu M, Drăguţ L. 2016. Random forest in remote sensing: a review of applications and future directions. ISPRS J Photogramm Remote Sens. 114:24–31. doi:10.1016/j.isprsjprs.2016. 01.011.
- Biah I, Azihou AF, Guendehou S, Sinsin B. 2024. Land use/land cover change and carbon footprint in tropical ecosystems in Benin, West Africa. Trees For People. 15:100488. doi:10. 1016/j.tfp.2023.100488.
- Boateng EY, Otoo J, Abaye DA. 2020. Basic tenets of classification algorithms K-nearest-neighbor, support vector machine, random forest and neural network: a review. JDAIP. 08(04): 341–357. doi:10.4236/jdaip.2020.84020.
- Breiman L. 2001. Random forests. Mach Learn. 45(1):5-32. doi:10.1023/A:1010933404324.
- Chabi A, Lautenbach S, Orekan VOA, Kyei-Baffour N. 2016. Allometric models and above-ground biomass stocks of a West African Sudan Savannah watershed in Benin. Carbon Balance Manage. 11(1), 1–18. doi:10.1186/s13021-016-0058-5.
- Congalton RG, Green K. 2008. Assessing the Accuracy of Remotely Sensed Data: Principles and Practices (Second Edition). CRC Press. 10.1201/9781420055139
- Fang G, Xu H, Yang SI, Lou X, Fang L. 2023. Synergistic use of Sentinel-1, Sentinel-2, and Landsat 8 in predicting forest variables. Ecol Indic. 151:110296. doi:10.1016/j.ecolind.2023. 110296.



- Farr T G, Rosen P A, Caro E, Crippen R, Duren R, Hensley S, Kobrick M, Paller M, Rodriguez E, Roth L, et al. 2007. The shuttle radar topography mission. Rev. Geophys. 45(2):1-33. doi:10.1029/2005RG000183.
- Ferreira V, Almazán-Gómez MÁ, Nechifor V, Ferrari E. 2022. The role of the agricultural sector in Ghanaian development: a multiregional SAM-based analysis. J Econ Struct. 11(1):6. doi:10.1186/s40008-022-00265-9.
- Foody GM. 2002. Status of land cover classification accuracy assessment. Remote Sens Environ. 80(1):185-201. www.elsevier.com/locate/rse. doi:10.1016/S0034-4257(01)00295-4.
- Forkuor G, Conrad C, Thiel M, Zoungrana BJB, Tondoh JE. 2017. Multiscale remote sensing to map the spatial distribution and extent of cropland in the sudanian savanna of West Africa. Remote Sens (Basel). 9(8):839. doi:10.3390/rs9080839.
- Freitas A, Dias JM, Lopes CL. 2024. Application of remote sensing methods for monitoring extent, condition and blue carbon storage in salt marshes. Remote Sens Appl Soc Environ. 35:101226. doi:10.1016/j.rsase.2024.101226.
- Gargiulo M, Dell'Aglio DAG, Iodice A, Riccio D, Ruello G. 2020. Integration of sentinel-1 and sentinel-2 data for land cover mapping using W-net. Sensors. 20(10):2969.doi:10.3390/ s20102969.
- Gessner U, Machwitz M, Esch T, Tillack A, Naeimi V, Kuenzer C, Dech S. 2015. Multi-sensor mapping of West African land cover using MODIS, ASAR and TanDEM-X/TerraSAR-X data. Remote Sens Environ. 164:282-297. doi:10.1016/j.rse.2015.03.029.
- Ghrefat H, Awawdeh M, Howari F, Al-Rawabdeh A. 2023. Chapter 12 Mineral exploration using multispectral and hyperspectral remote sensing data. In: Stathopoulos N, Tsatsaris A, Kalogeropoulos K, editors. Geoinformatics for geosciences. Amsterdam, Netherlands: Elsevier; p. 197-222. doi:10.1016/B978-0-323-98983-1.00013-2.
- Grégoire JM, Eva HD, Belward AS, Palumbo I, Simonetti D, Brink A. 2013. Effect of landcover change on Africa's burnt area. Int J Wildland Fire. 22(2):107-120. doi:10.1071/ WF11142.
- Gregorio A, Di Henry M, Donegan E, Finegold Y, Latham J, Jonckheere I, Cumani R. 2016. Classification concepts land cover classification system software version 3. www.fao.org/.
- Gregorio A, Jansen LJM. 2000. Land cover classification system (LCCS). Software Version 1.0. https://www.fao.org/3/x0596e/x0596e00.htm.
- Habib A, Al-Ruzouq R, Kim C, Habib AF, Al-Ruzouq RI, Kim CJ. 2004. Semi-automatic registration and change detection using multi source imagery with varying geometric and radiometric properties. PS ICWG II/IV Change Detection and Updating for Geodatabase. https:// www.researchgate.net/publication/254287460.
- He D, Liu X, Shi Q, Zheng Y. 2025. Visual-language reasoning segmentation (LARSE) of function-level building footprint across Yangtze River Economic Belt of China. Sustain Cities Soc. 127:106439. doi:10.1016/j.scs.2025.106439.
- He D, Shi Q, Xue J, Atkinson PM, Liu X. 2023. Very fine spatial resolution urban land cover mapping using an explicable sub-pixel mapping network based on learnable spatial correlation. Remote Sens Environ. 299:113884. doi:10.1016/j.rse.2023.113884.
- Hosseini MM, Valadan Zoej MJ, Taheri Dehkordi A, Ghaderpour E. 2024. Cropping intensity mapping in Sentinel-2 and Landsat-8/9 remote sensing data using temporal transfer of a stacked ensemble machine learning model within Google earth engine. Geocarto Int. 39(1), 1-28. doi:10.1080/10106049.2024.2387786.
- Houghton RA, Hackler JL. 2006. Emissions of carbon from land use change in sub-Saharan Africa. J Geophys Res. 111(G2), 1-12. doi:10.1029/2005JG000076.
- Huete AR. 1988. A soil-adjusted vegetation index (SAVI). Remote Sens Environ. 25(3):295-309. doi:10.1016/0034-4257(88)90106-X.
- Ibrahim S. 2023. Improving land use/cover classification accuracy from random forest feature importance selection based on synergistic use of sentinel data and digital elevation model in agriculturally dominated landscape. Agriculture (Switzerland). 13(1):98. doi:10.3390/ agriculture13010098.

- Inglada J, Vincent A, Arias M, Marais-Sicre C. 2016. Improved early crop type identification by joint use of high temporal resolution SAR and optical image time series. Remote Sens (Basel), 8(5):362, doi:10.3390/rs8050362.
- Irfan A, Li Y, E X, Sun G. 2025. Land use and land cover classification with deep learningbased fusion of SAR and optical data. Remote Sens (Basel). 17(7):1298. doi:10.3390/ rs17071298.
- Islam KI, Elias E, Carroll KC, Brown C. 2023. Exploring random forest machine learning and remote sensing data for streamflow prediction: an alternative approach to a process-based hydrologic modeling in a snowmelt-driven watershed. Remote Sens (Basel). 15(16):3999. doi:10.3390/rs15163999.
- Jansen A, Robertson A, Leigh T, Andrea W. 2005. Rapid appraisal of riparian condition. In: River and riparian land management technical guideline (Vol. 4A, pp.1-16). Land & Water Australia.
- Jorge F, Mutwale-Mutale N, Sandhage-Hofmann A, Braun M, Cambule A, Nhantumbo A, Chabala LM, Shepande C, Chishala B, Lisboa S, et al. 2025. Anthropogenic disturbances superimpose climate effects on soil organic carbon in savanna woodlands of sub-Saharan Africa. Glob Biogeochem Cycl. 39(2), 1-24. doi:10.1029/2023GB008086.
- Joshi N, Mitchard ETA, Woo N, Torres J, Moll-Rocek J, Ehammer A, Collins M, Jepsen MR, Fensholt R. 2015. Mapping dynamics of deforestation and forest degradation in tropical forests using radar satellite data. Environ Res Lett. 10(3):034014. doi:10.1088/1748-9326/10/3/ 034014.
- Kior A, Sukhov V, Sukhova E. 2021. Application of reflectance indices for remote sensing of plants and revealing actions of stressors. Photonics. 8(12):582 doi:10.3390/photonics8120582.
- Lee J, Kim K, Lee K. 2024. Multi-sensor image classification using the random forest algorithm in Google Earth engine with KOMPSAT-3/5 and CAS500-1 images. Remote Sens (Basel). 16(24):4622. doi:10.3390/rs16244622.
- Lu D, Batistella M, Li G, Moran E, Hetrick S, Freitas CdC, Dutra LV, Sant'anna SJS. 2012. Land use/cover classification in the Brazilian Amazon using satellite images. Pesqui Agropecu Bras. 47(9):1185–1208. doi:10.1590/S0100-204X2012000900004.
- Malamiri HRG, Zare H, Rousta I, Olafsson H, Verdiguier EI, Zhang H, Mushore TD. 2020. Comparison of harmonic analysis of time series (HANTS) and multi-singular spectrum analysis (M-SSA) in reconstruction of long-gap missing data in NDVI time series. Remote Sens (Basel). 12(17):2747. doi:10.3390/rs12172747.
- Mbow C. 2020. Use it sustainably or lose it! The land stakes in SDGs for sub-Saharan Africa. Land (Basel). 9(3):63. doi:10.3390/land9030063.
- Mohammed FG. 2013. Satellite image gap filling technique. Int J Adv Res Technol. 2, 348-351. Mountrakis G, Im J, Ogole C. 2011. Support vector machines in remote sensing: a Review. ISPRS J Photogramm Remote Sens. 66(3):247-259. doi:10.1016/j.isprsjprs.2010.11.001.
- Nhemaphuki D, Chetri KT, Shrestha S. 2020. Fusion of radar and optical data for land cover classification using machine learning approach. J Geoinformatics, Nep. 20(1):39-45. doi:10. 3126/njg.v20i1.39476.
- Olasunkanmi N, Magawata U, Bayowa OG. 2023. Assessment of image ratio technique: Targeting structural features and mineralization characteristics in the southwestern part of the Sokoto Basin in Nigeria using Landsat 8 imagery. Kuwait J Sci. 50(4):803-811. doi:10. 1016/i.kis.2023.02.030.
- Onačillová K, Gallay M, Paluba D, Péliová A, Tokarčík O, Laubertová D. 2022. Combining landsat 8 and sentinel-2 data in Google Earth engine to derive higher resolution land surface temperature maps in urban environment. Remote Sens (Basel). 14(16):4076. doi:10.3390/ rs14164076.
- Onyeaka H, Siyanbola KF, Akinsemolu AA, Tamasiga P, Mbaeyi-Nwaoha IE, Okonkwo CE, Odeyemi OA, Oladipo EK. 2024. Promoting equity and justice: harnessing the right to food for Africa's food security. Agric Food Secur. 13(1), 1-26. doi:10.1186/s40066-024-00505-0.



- Osborne CP, Charles-Dominique T, Stevens N, Bond WJ, Midgley G, Lehmann CER. 2018. Human impacts in African savannas are mediated by plant functional traits. New Phytol. 220(1):10-24. doi:10.1111/nph.15236.
- Pastick NJ, Dahal D, Wylie BK, Parajuli S, Boyte SP, Wu Z. 2020. Characterizing land surface phenology and exotic annual grasses in dryland ecosystems using landsat and sentinel-2 data in harmony. Remote Sens (Basel). 12(4):725. doi:10.3390/rs12040725.
- Repetto R, Holmes T. 1983. The role of population in resource depletion in developing countries. Popul Dev Rev. 9(4):609-632. doi:10.2307/1973542.
- Rodriguez-Galiano VF, Ghimire B, Rogan J, Chica-Olmo M, Rigol-Sanchez JP. 2012. An assessment of the effectiveness of a random forest classifier for land-cover classification. ISPRS J Photogramm Remote Sens. 67:93–104. doi:10.1016/j.isprsjprs.2011.11.002.
- Sahadevan DK, Sitiraju S, Sharma J. 2013. Radar vegetation index as an alternative to NDVI for monitoring of soyabean and cotton. Indian Cartographer, 33, 91-96.
- Seleim AM, Bekiet MH, Hammed MS. 2022. Enhanced lithological mapping of Durba-Araba basement blocks, along the eastern margin of the Central Gulf of Suez Rift, Egypt, using Landsat-8 Data. Arabian J. Geosci. 15(14):1-18. 10.1007/s12517-022-10208-0.
- Shahi AP, Rai PK, Mishra VN. 2023. Chapter 5 Remote sensing data extraction and inversion techniques: a review. In: Kumar Singh A, Tiwari S, editors. Atmospheric remote sensing (pp. 85–104). Amsterdam, Netherlands: Elsevier. doi:10.1016/B978-0-323-99262-6.00021-3.
- Shawky M, Moussa A, Hassan QK, El-Sheimy N. 2019. Pixel-based geometric assessment of channel networks/orders derived from global spaceborne digital elevation models. Remote Sens (Basel). 11(3):235. doi:10.3390/rs11030235.
- Sheykhmousa M, Mahdianpari M, Ghanbari H, Mohammadimanesh F, Ghamisi P, Homayouni S. 2020. Support vector machine versus random forest for remote sensing image classification: a meta-analysis and systematic review. IEEE J Sel Top Appl Earth Observ Rem Sens. 13:6308-6325. doi:10.1109/JSTARS.2020.3026724.
- Shivakumar BR, Rajashekararadhya SV. 2018. An investigation on land cover mapping capability of classical and fuzzy based maximum likelihood classifiers. Int J Eng Technol. 7(2):939. doi:10.14419/ijet.v7i2.10743.
- Sobrino JA, Jiménez-Muñoz JC, Paolini L. 2004. Land surface temperature retrieval from LANDSAT TM 5. Remote Sens Environ. 90(4):434-440. doi:10.1016/j.rse.2004.02.003.
- Sonawane MS, Dhawale CA. 2016. Evaluation and analysis of few parametric and nonparametric classification methods. 2016 second international conference on computational intelligence & communication technology (CICT); p. 14-21. doi:10.1109/CICT.2016.13.
- Stumberg N, Hauglin M, Bollandsås O, Gobakken T, Næsset E. 2014. Improving classification of airborne laser scanning echoes in the forest-tundra ecotone using geostatistical and statistical measures. Remote Sens (Basel). 6(5):4582-4599. doi:10.3390/rs6054582.
- Tallón-Ballesteros AJ, Riquelme JC. 2014. Data mining methods applied to a digital forensics task for supervised machine learning; p. 413-428. Cham, Switzerland: Springer Nature. doi: 10.1007/978-3-319-05885-6\_17.
- Tassi A, Gigante D, Modica G, Di Martino L, Vizzari M. 2021. Pixel-vs. Object-based landsat 8 data classification in google earth engine using random forest: the case study of Maiella National Park. Remote Sens (Basel). 13(12):2299. doi:10.3390/rs13122299.
- Umoh UA, Eyoh IJ, Nyoho EE, Murugesan VS. 2022. Fuzzy-machine learning models for the prediction of fire outbreaks: A comparative analysis. In: Artificial intelligence and machine learning for EDGE computing (pp. 207-233). London, UK: Elsevier. doi:10.1016/B978-0-12-824054-0.00025-3.
- Villa P, Mousivand A, Bresciani M. 2014. Aquatic vegetation indices assessment through radiative transfer modeling and linear mixture simulation. Int J Appl Earth Obs Geoinf. 30:113-127. doi:10.1016/j.jag.2014.01.017.
- Wang Q, Atkinson PM. 2018. Spatio-temporal fusion for daily Sentinel-2 images. Remote Sens. Environ. 204:31-42. doi:10.1016/j.rse.2017.10.046.



- Wang Q, Wang L, Zhu X, Ge Y, Tong X, Atkinson PM. 2022. Remote sensing image gap filling based on spatial-spectral random forests. Sci Rem Sens. 5:100048. doi:10.1016/j.srs.2022. 100048.
- Wu C, Niu Z, Gao S. 2012. The potential of the satellite derived green chlorophyll index for estimating midday light use efficiency in maize, coniferous forest and grassland. Ecol Indic. 14(1):66-73. doi:10.1016/j.ecolind.2011.08.018.
- Xu H. 2006. Modification of normalized difference water index (NDWI) to enhance open water features in remotely sensed imagery. Int J Rem Sens. 27(14):3025-3033. doi:10.1080/ 01431160600589179.
- Yan L, Roy DP. 2018. Large-area gap filling of landsat reflectance time series by spectralangle-mapper based spatio-temporal similarity (SAMSTS). Remote Sens (Basel). 10(4):609. doi:10.3390/rs10040609.
- Yangouliba GI, Zoungrana BIB, Hackman KO, Koch H, Liersch S, Sintondii LO, Dipama IM, Kwawuvi D, Ouedraogo V, Yabré S, et al. 2022. Modelling past and future land use and land cover dynamics in the Nakambe River Basin, West Africa. Model Earth Syst Environ. 9(2):1651-1667. doi:10.1007/s40808-022-01569-2.
- Zhang H, Zhang Yao, Gao T, Lan Shu, Tong F, Li M. 2023. Landsat 8 and sentinel-2 fused dataset for high spatial-temporal resolution monitoring of farmland in china's diverse latitudes. Remote Sensing. 15(11):2951 doi:10.3390/rs15112951.
- Zoungrana BJ-B, Dimobé K. 2023. NDVI-derived vegetation trends and driving factors in west african sudanian savanna. AJPS. 14(10):1130-1145. doi:10.4236/ajps.2023.1410077.